ACS Catalysis

Research Article

Cite This: ACS Catal. 2018, 8, 8336–8345

pubs.acs.org/acscatalysis

Hydroclassified Combinatorial Saturation Mutagenesis: Reshaping Substrate Binding Pockets of *Kp*ADH for Enantioselective Reduction of Bulky−Bulky Ketones

Guo-Chao Xu,[†] Yue Wang,[†] Ming-Hui Tang,[†] Jie-Yu Zhou,[†] Jing Zhao,[‡] Rui-Zhi Han,[†] and Ye Ni*[,†]

[†]Key Laboratory of Industrial Biotechnology, Ministry of Education, School of Biotechnology, Jiangnan University, Wuxi 214122, Jiangsu, China

[‡]Key Laboratory of Systems Microbial Biotechnology, Tianjin Institute of Industrial Biotechnology, Chinese Academy of Sciences, Tianjin 300308, China

Supporting Information

ABSTRACT: A hydroclassified combinatorial saturation mutagenesis (HCSM) strategy was proposed for reshaping the substrate binding pocket by dividing 20 amino acids into four groups based on their hydrophobicity and size. These smart HCSM libraries could significantly reduce screening effort especially for the simultaneous mutagenesis of three or more residues and lacking high throughput screening methods. Employing HCSM strategy, the stereoselectivity of *Kp*ADH, an alcohol dehydrogenase from *Kluyveromyces polysporus*, was efficiently improved to 99.4% *ee*. (4-Chlorophenyl)(pyridin-2-yl)methanone (CPMK), generally regarded as a "hard-to-reduce" ketone, was used as a model substrate, and its corresponding chiral alcohol products could be utilized as antihistamine precursors. The best variant 50C10 displayed higher binding affinity and catalytic efficiency toward CPMK with K_M/k_{cat} of 59.3 $s^{-1}\cdot mM^{-1}$, 3.51-fold that of *Kp*ADH. Based on MD simulations, increased difference between two binding pockets, enhanced hydrophobicity, and $\pi-\pi$ and halogen−alkyl interactions were proposed to favor the enantioselective recognition and substrate binding in 50C10. Substrate spectrum analysis revealed that 50C10 exhibited improved enantioselectivity toward diaryl ketones especially with halo- or other electron-withdrawing groups. As much as 500 mM CPMK could be asymmetrically reduced into chiral diaryl alcohols with *ee* of 99.4% and a space−time yield of 194 $g\cdot L^{-1}\cdot d^{-1}$ without addition of external $NADP^+$. This study provides an effective mutagenesis strategy for the protein engineering of substrate specificity and enantioselectivity.

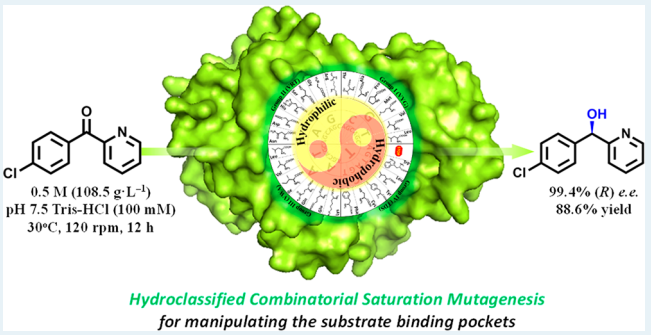

KEYWORDS: *alcohol dehydrogenase, hydroclassified amino acids, directed evolution, enantioselectivity, (R)-CPMA*

INTRODUCTION

Optically active diarylmethanols are important building blocks and structural motifs of pharmaceuticals, such as antihistamine, diuretic, antiepileptic, asthma, and antidepressant drugs (Scheme 1).[1] Moreover, via S_N2 substitution at the C−O bond, chiral diarylmethanols could be facilely converted into diarylmethane derivatives without loss of optical purity.[2] As a result, efficient synthesis of chiral diarylmethanols, typically through asymmetric addition of aryl nucleophiles benzaldehyde or asymmetric transfer hydrogenation (ATH) of the corresponding diaryl ketones, is of special interest.[3]

Compared with ATH using precious metals, such as iridium, rhodium, and ruthenium as catalysts, carbonyl reductases mediated reactions have many inherent merits such as environmental compatibility, high enantioselectivity, and mild reaction conditions.[4] Thus, asymmetric bioreduction has attracted ever-increasing attention, and various reductases/dehydrogenases have been validated at large scale.[5] However, the enantioselective reduction of bulky−bulky diaryl ketones with two similar aryl substituents remains challenging for not only chemocatalysts but also biocatalysts, especially at high substrate loading.[6] Only SSCR from *Sporobolomyces salmonicolor* and commercial ketoreductase KRED124 have been reported with 88−94% *ee* at 10 $g\cdot L^{-1}$ (4-chlorophenyl)-(pyridin-2-yl)methanone (CPMK, **1a**) in depletion of 1 $g\cdot L^{-1}$ $NADP^+$.[7] Previously, *Kp*ADH has been identified from *Kluyveromyces polysporus* by genome database mining with 82.5% (*R*) *ee* in the reduction of 100 mM CPMK.[8] The *Kp*ADH displays the highest k_{cat}/K_M among all the reported reductases, indicating it is a promising candidate for further protein engineering.

Directed evolution is a commonly practiced approach for protein engineering as an alternative to rational design.[9] Site-directed saturation mutagenesis is a major strategy performed

Received: June 22, 2018
Revised: July 26, 2018

DOI: 10.1021/acscatal.8b02286
ACS Catal. 2018, 8, 8336−8345

Scheme 1. Stereoview of the Homology Structure of *Kp*ADH and Asymmetric Reduction of CPMK into (*R*)-CPMA Catalyzed by *Kp*ADH. (A) Homology Structure of *Kp*ADH; (B) Asymmetric Reduction of CPMK into (*R*)-CPMA; (C) Residues Lining the Substrate Binding Pockets[a]

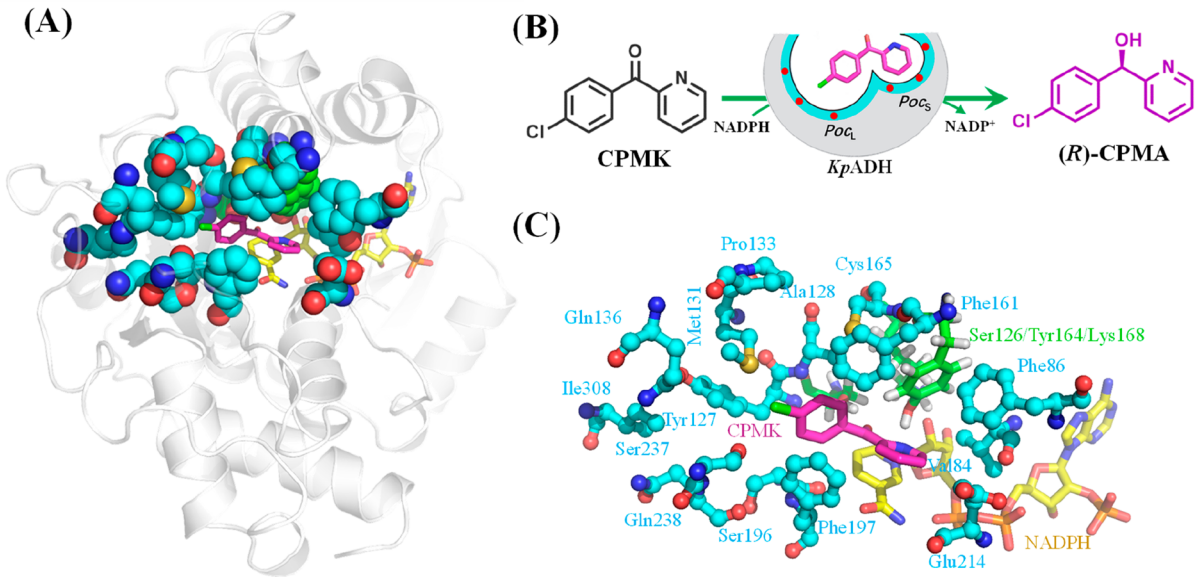

[a]Catalytic triad illustrated in green stick, NADPH in yellow stick, CPMK in magenta stick, residues of substrate binding pockets in cyan ball and stick.

Scheme 2. Hydroclassified Combinatorial Saturation Mutagenesis Alphabets and the Screening Effort Required for Combinatorial Saturation Mutagenesis of Two or Three Residues Employing NNK/S, 22c-Trick, and HCSM Strategies[a]

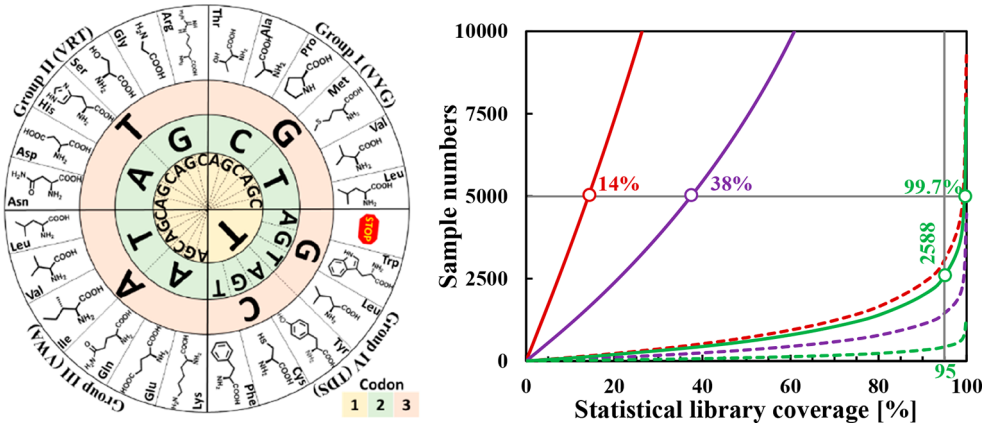

[a]Dashed lines, 2 residues; solid lines, 3 residues; red lines, NNK/S; purple lines, 22c-trick; green lines, HCSM. Number of variants is calculated according to the formula $L = -V \times \mathrm{Ln}(1 - F)$, where L is the number of variants or library size, V is the theoretical number of variants, and F is the expected coverage of library, e.g., 0.95 for 95% coverage.

at sites lining the binding pockets of enzymes to improve their limited substrate scope, insufficient activity, and poor regio- or stereoselectivity.[10] Although numerous successes in obtaining enzymes with improved catalytic properties have been achieved by directed evolution, many uncertainties still persist to be clarified, for example, how to group a variety of residues into randomization site, how to choose optimal upward pathways, etc.[11] As the number of residues in a randomization site increases to five or more, the screening effort for 95% library coverage, as calculated by CASTER based on the Patrick/Firth algorithm, is astronomically high.[12] Therefore, the construction of libraries for multiple sites with reasonable size is still challenging, especially in the engineering of certain properties, such as stereoselectivity, for which a high-throughput screening method is not available.[13] To solve the labor-intensive bottleneck, three tricks have been proposed to create "smart" mutant libraries: (1) binary patterning method employing polar/nonpolar residues, (2) splitting up a large number of sites into smaller ones followed by iterative saturation mutagenesis, and (3) use of reduced amino acid alphabets.[14] NNK (32:20, codons:amino acids), NDT (12:12), or 22c-trick (22:20) degeneracy have been commonly adopted in directed evolution to search the whole protein sequence space.[15] However, the concurrent oversampling increases as the residues in randomization site increase from one residue to more, and the inevitable codon bias emerges with the redundant degenerated codons. In the simultaneous mutation of three residues as illustrated in Scheme 2, the coverage rates of 2000−3000 variants (generally accepted screening work for enantioselectivity engineering) are 14% and 38% for NNK and

DOI: 10.1021/acscatal.8b02286
ACS Catal. 2018, 8, 8336−8345

22c-trick, respectively, far below 95% library coverage. Two new approaches, the smallest amino acids alphabet and triple-codon saturation mutagenesis, have been developed to construct smaller but smarter libraries for reduced screening work.[16] Nevertheless, the diversity is limited and most of the variants might be deactivated, especially in the case of simultaneous mutation of five or more sites.[17]

Herein, a new strategy, hydroclassified combinatorial saturation mutagenesis (HCSM), was proposed to facilely engineer the enantioselectivity of an alcohol dehydrogenase from *Kluyveromyces polysporus* (*Kp*ADH) (Scheme 2) based on the homology model. Residues lining the binding pockets were divided into groups and subjected to combinatorial saturation mutagenesis employing reduced amino acids alphabet based on hydrophobicity and steric hindrance. With regard to the simultaneous mutation of three residues, only 2588 variants are required for 95% coverage. This study provides evidence for the feasibility of this HCSM strategy by enhancing the enantioselectivity of *Kp*ADH from 82.5% to 99.4%. The beneficial variant of *Kp*ADH also exhibited high catalytic efficiency and could be applied in the preparation of optically active diaryl alcohols at as high as 500 mM substrate loading.

RESULTS AND DISCUSSION

Alanine and Tyrosine Scanning for Hotspots. A proposed mechanism for asymmetric carbonyl reduction catalyzed by short chain dehydrogenase/reductase (SDR) has been well reviewed with Ser-Tyr-Lys as catalytic triad.[18] Catalytic residues Ser and Tyr are responsible for the stabilization of alkoxide formed on hydride transfer from NADPH and nucleophilic attack, while Lys is essential for the stabilization of substrate and activation of water. It has been recognized that there are small and large binding pockets (Poc_S and Poc_L) in SDR which could discriminate and accommodate prochiral ketones with substituents differing in size.[19] Physical and chemical properties of Poc_S and Poc_L, determined by their residues constitution, are vital for catalytic properties, especially substrate specificity and enantioselectivity. A homology model of *Kp*ADH was constructed employing crystal structures of methylglyoxal/isovaleraldehyde reductase from *Saccharomyces cerevisiae* (51% identity, PDB: 4PVC) and ketoreductase 1 from *Candida glabrata* (50% identity, PDB: 5B6K) as templates.[20] Evaluation of the homology model of *Kp*ADH reveals that over 99.4% of residues are located in the allowable regions in the Ramachandran plot (Figure S1). The proposed substrate binding pockets of *Kp*ADH are made up of 16 residues according to its homology model, including V84, F86, Y127, A128, M131, P133, Q136, F161, C165, S196, F197, E214, S237, T234, Q238, and I308 (Table 1). Simultaneous saturation mutagenesis of all the residues in substrate binding pockets is obviously beyond reach. Moreover, most of the above 16 residues locate in the loop region and might not be correctly assigned into Poc_S or Poc_L according to the homology model. As a result, we attempted to identify the hotspots by alanine and tyrosine scanning and then classify them into Poc_S or Poc_L, which were presumed to accommodate 2′-pyridyl and 4′-chlorophenyl groups of CPMK, respectively. Mutation of Poc_S residues into larger amino acids might cause a reduction in the size of Poc_S and thus increased volumetric difference between Poc_S and Poc_L, whereas mutation into smaller amino acids could lead to enlarged Poc_S and decreased difference between two pockets. Presumably, variants with mutations at Poc_S residues into larger amino acids might exhibit higher enantioselectivity than mutations into smaller amino acids. Likewise, variants with mutation at Poc_L residues into smaller amino acids might exhibit higher enantioselectivity than mutations into larger amino acids.

Table 1. Alanine/Tyrosine Scanning of *Kp*ADH toward CPMK

residue	*ee* of alanine mutation (%)	*ee* of tyrosine mutation (%)
F86	82.7 ± 0.3	75.6 ± 0.5
Y127	78.7 ± 0.6	82.5 ± 0.6 (77.9 ± 0.5)[a]
A128	82.5 ± 0.6	82.9 ± 0.3 (82.8 ± 0.2)[a]
M131	88.6 ± 0.3	86.7 ± 0.5
P133	85.3 ± 0.7	82.7 ± 0.3
Q136	78.3 ± 0.8	79.7 ± 0.3
F161	67.6 ± 0.5	67.5 ± 0.3
C165	75.5 ± 0.3	88.1 ± 0.5
S196	74.7 ± 0.5	74.7 ± 0.3
F197	94.2 ± 0.5	86.6 ± 0.5
E214	79.8 ± 0.3	93.8 ± 0.2
S237	96.1 ± 0.6	94.1 ± 0.4
Q238	79.3 ± 0.2	87.7 ± 0.5
T234	82.1 ± 0.5	83.7 ± 0.3
I308	76.8 ± 0.3	73.4 ± 0.4

[a]Number in the parentheses denotes the *ee* of mutants with phenylalanine mutation.

Preliminary screening was therefore performed by mutation of each residue into alanine and tyrosine (namely alanine and tyrosine scanning method),[21] due to their moderate hydrophobicity (+1.8 for alanine and −1.3 for tyrosine), different size, and additional hydroxyl group of tyrosine. Scanning results revealed that 11 residues participate in influencing the enantioselectivity of *Kp*ADH toward CPMK, while the other five residues V84, F86, A128, P133, and T234 were eliminated due to their unstable *ee* of 15−83% (V84, data not shown) or similar *ee* values compared with *Kp*ADH (Table 1). As shown in Table 1, variants with mutations at residues Y127, Q136, F161, and S196 exhibited similar enantioselectivity between alanine and tyrosine mutations. As a result, they were not selected as hotspots, in spite of their different enantioselectivity in comparison with *Kp*ADH. The *ee* values of I308A and I308Y were 76.8% and 73.4% respectively, lower than 82.5% *ee* of *Kp*ADH. Thus, site 308 was also not chosen as a hotspot. Mutations at M131, C165, F197, E214, S237, and Q238 resulted in highly improved *ee*. Hence, these six sites were selected as mutational hotspots. The alanine mutants M131A (88.6%), F197A (94.2%), and S237A (96.1%) exhibited higher *ee* values than their corresponding tyrosine mutants M131Y (86.7%), F197Y (86.6%), and S237Y (94.1%), respectively. The results suggest that M131, F197, and S237 could be vital sites in Poc_L due to their enhanced stereoselectivity when mutated into smaller amino acids. The alanine mutants C165A (75.5%), E214A (79.8%), and Q238A (79.3%) displayed lower *ee* values than their corresponding tyrosine mutants C165Y (88.1%), E214Y (93.8%), and Q238Y (87.7%), respectively. It indicates that C165, E214, and Q238 could be key sites in Poc_S since higher *ee* values were achieved when mutated into larger amino acids. Consequently, six hotspots were identified to play critical roles in manipulating the enatioselectivity of *Kp*ADH, and they were grouped into Poc_S and Poc_L residues for further study.

Development and Screening of HCSM Libraries. Considering that the enantioselectivity could be manipulated

DOI: 10.1021/acscatal.8b02286
ACS Catal. 2018, 8, 8336−8345

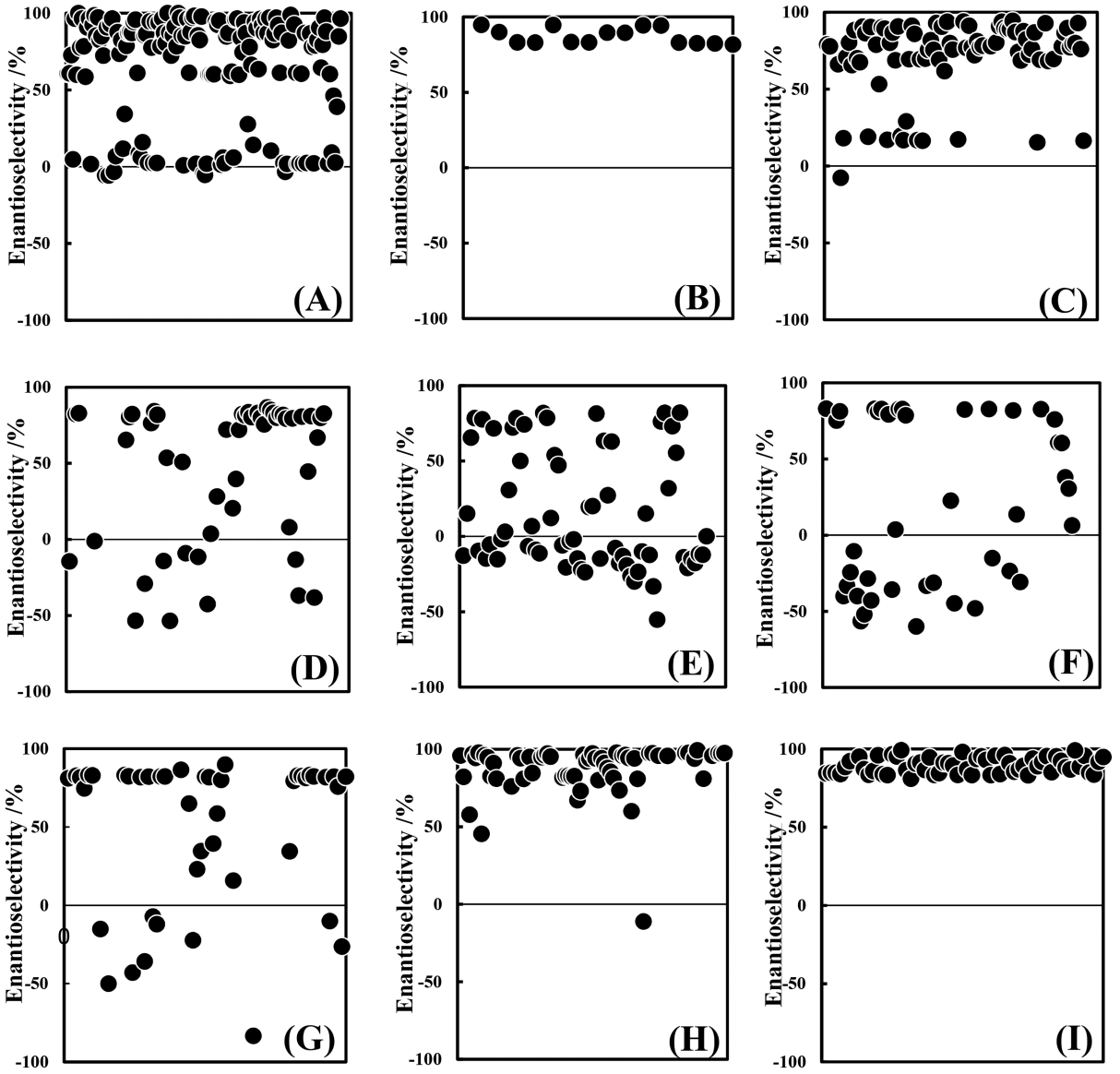

Figure 1. Screening results of HCSM libraries on large and small substrate binding pockets. (A) Poc_L-I, (B) Poc_L-II, (C) Poc_L-III, (D) Poc_L-IV, (E) Poc_S-I, (F) Poc_S-II, (G) Poc_S-III, (H) Poc_S-IV, and (I) combinatorial mutagenesis.

by more than one residue in substrate binding pockets, combinatorial mutagenesis is often performed. To conduct the combinatorial saturation mutagenesis with high efficacy, hydroclassified amino acid alphabet was proposed by classifying the codons into four groups based on the codon bias of *E. coli*, hydrophobicity, and size of amino acids. As illustrated in Scheme 2, 24 codons were chosen for 20 amino acids and were classified into Group I (designated as "Hydrophobic group", VYG), Group II ("Hydrophilic group", VRT), Group III ("Mixed group", VWA), and Group IV ("Aromatic group", TDS). Specifically, Group I codes for threonine, methionine, alanine, valine, proline, and leucine. Group II codes for aspartate, asparagine, serine, glycine, histidine, and arginine. Group III codes for lysine, isoleucine, glutamate, valine, glutamine, and leucine. Group IV codes for tyrosine, tryptophan, phenylalanine, cysteine, leucine, and stop codons. Saturation mutagenesis employing this hydroclassified amino acid alphabet is named as hydroclassified combinatorial saturation mutagenesis (HCSM). Compared with other combinatorial mutagenesis strategies for engineering enantioselectivity such as triple-codon saturation mutagenesis (TCSM), double-codon saturation mutagenesis (DCSM), and single-codon saturation mutagenesis (SCSM), HCSM is a hexatruple-codon saturation mutagenesis method in which each site is mutated into six other amino acids. It is therefore supposed to be more efficient since more codons are employed in randomizing the mutation sites (TCSM > DCSM > SCSM).[22] Most importantly, in HCSM, all hotspots could be simultaneously mutated into hydrophobic (Group I), hydrophilic (Group II), or aromatic (Group IV) amino acids, as well as the mixed hydrophobic and hydrophilic codons in Group III, which could conduce to the evaluation of possible synergistic effects of hydrophobicity and hydrophilicity. Consequently, HCSM is advantageous for developing libraries with high diversity in volume, hydrophobicity, substituents, and electricity.

Results of HCSM Libraries in Poc_L. Furthermore, the HCSM libraries of *Kp*ADH at the above six hotspots in Poc_S and Poc_L were constructed. For M131, F197, and S237 in Poc_L, all three sites were combinatorial saturation mutated adopting the

DOI: 10.1021/acscatal.8b02286
ACS Catal. 2018, 8, 8336−8345

Table 2. Kinetic Parameters of *Kp*ADH and Variants toward CPMK

variant	library	mutation	*ee* (%)	K_M (mM)	k_{cat} (s^{-1})	k_{cat}/K_M ($s^{-1}\cdot mM^{-1}$)
*Kp*ADH	–	–	82.5 ± 0.5	0.78 ± 0.07	13.2 ± 0.3	16.9
3D3	Poc_L-I	M131A/F197T/S237A	98.2 ± 0.3	3.84 ± 0.11	8.23 ± 0.17	2.14
3H8	Poc_L-I	M131A/S237A	97.8 ± 0.4	1.95 ± 0.10	21.3 ± 0.4	10.9
6C12	Poc_L-I	M131V/F197T/S237A	98.5 ± 0.3	2.75 ± 0.15	12.7 ± 0.5	4.62
43D11	Poc_S-IV	C165F/E214Y/Q238C	97.4 ± 0.5	1.51 ± 0.08	15.8 ± 0.4	10.46
45A3	Poc_S-IV	C165F/E214Y	97.5 ± 0.3	0.68 ± 0.05	14.9 ± 0.5	21.91
47G9	Poc_S-IV	C165W/E214Y/Q238C	97.7 ± 0.5	1.46 ± 0.09	13.2 ± 0.4	9.04
49A7	Comb. Lib.[a]	M131V/F197T/E214Y/S237A	98.9 ± 0.2	1.88 ± 0.07	28.4 ± 0.5	15.1
49D6	Comb. Lib.	C165W/E214Y/S237A/Q238C	98.9 ± 0.3	2.62 ± 0.08	22.0 ± 0.3	8.40
50C10	Comb. Lib.	C165F/E214Y/S237A	99.4 ± 0.2	0.35 ± 0.05	20.8 ± 0.3	59.4
51E10	Comb. Lib.	M131A/C165F/F197T/E214Y/S237A	98.7 ± 0.4	6.52 ± 0.13	55.4 ± 1.2	8.50
M131V	SDM[b]	M131V	87.4 ± 0.6	1.14 ± 0.07	9.39 ± 0.21	8.24
C165F	SDM	C165F	89.1 ± 0.3	0.52 ± 0.04	9.26 ± 0.22	17.8
F197T	SDM	F197T	87.4 ± 0.5	8.12 ± 0.13	6.80 ± 0.19	0.84
E214Y	SDM	E214Y	94.2 ± 0.3	0.80 ± 0.06	14.9 ± 0.6	18.6
S237A	SDM	S237A	96.1 ± 0.3	0.38 ± 0.04	15.4 ± 0.7	40.5
Q238C	SDM	Q238C	88.4 ± 0.3	3.42 ± 0.14	10.2 ± 0.3	2.98

[a]Comb. Lib.: combinatorial mutagenesis library. [b]SDM: site-directed mutagenesis.

hydroclassified amino acid alphabet (Groups I, II, III, and IV) to generate HCSM libraries of Poc_L-I, Poc_L-II, Poc_L-III, and Poc_L-IV, respectively. Theoretically, at least 647 variants are required for each library to achieve 95% coverage according to the formula in Scheme 2. In total, at least 2588 variants are required for four libraries of Poc_L. This library size is still too large for enantioselectivity analysis by chiral HPLC. As a result, two rounds of screening were adopted to isolate *Kp*ADH variants with both high activity and enantioselectivity. First, deactivated variants were eliminated by high throughput screening on activity. Then, biotransformation employing the active variants was conducted for enantioselectivity analysis. As shown in Figure 1B, 98% of the variants of Poc_L-II were deactivated, and only 15 variants displayed 82−94% *ee* and less than 50% activity of *Kp*ADH, indicating hydrophilic mutagenesis was not advantageous for the enantioselective binding and reduction of CPMK. Mutation of residues in Poc_L into aromatic amino acids resulted in less than 82% *ee* for all variants (Figure 1D), demonstrating that the decreased difference between size of Poc_S and Poc_L was unfavorable for the discrimination of 2′-pyridyl and 4′-chlorophenyl groups, which is in coincidence with the above hypothesis. Most variants of Poc_L-I and Poc_L-III were still active and exhibited higher *ee*, especially using Group I codons (Figure 1A, C). The three best variants in Poc_L-I, 3D3, 3H8, and 6C12, exhibited *ee* of 98.2%, 97.8%, and 98.5% respectively, significantly higher than that of *Kp*ADH (82.5% *ee*) (Table 2). Compared with Poc_L-II and Poc_L-III, hydrophobic mutagenesis could alleviate the severe deactivation caused by hydrophilic mutagenesis to some extent. Consequently, hydrophobic interaction was important for the large substrate binding pocket. All the variants with over 95% *ee* in four HCSM libraries of Poc_L were rescreened and sequenced as shown in the Supporting Information. The mutational sites in 3D3, 3H8, and 6C12 are M131A/F197T/S237A, M131A/S237A, and M131V/F197A/S237A, respectively.

Results of HCSM Libraries in Poc_S. Likewise, four HCSM libraries (Poc_S-I, Poc_S-II, Poc_S-III, and Poc_S-IV) of C165, E214, and Q238 of Poc_S were also developed and screened as shown in Figure 1E−H and Tables S3−S10. No severe deactivation was found in all four libraries. Variants with similar or higher specific activity toward CPMK than *Kp*ADH were selected for enantioselectivity analysis. Almost all the variants in Poc_S-I, Poc_S-II, and Poc_S-III displayed lower *ee* than *Kp*ADH as illustrated in Figure 1E−G. Unlike the importance of hydrophobic interaction observed in Poc_L, steric hindrance plays a critical role in Poc_S. It is noted that mutation of C165, E214, and Q238 into aromatic amino acids employing Group IV codons resulted in significantly improved *ee* (Figure 1H). The three best variants in Poc_S-IV, 43D11 (C165F/E214Y/Q238C), 45A3 (C165F/E214Y), and 47G9 (C165W/E214Y/Q238C), exhibited *ee* of 97.4%, 97.5%, and 97.7%, respectively. As expected, mutation of residues in Poc_S into larger amino acids would decrease the size of Poc_S and further increase the discrepancy between Poc_S and Poc_L, which is favorable for the enantioselective recognition of prochiral ketones.

Results of Combinatorial Mutagenesis of Poc_L and Poc_S. Combinatorial mutageneses at hotspots of Poc_S and Poc_L were performed by mixing 3D3, 5H4, 6C12, 43D11, 45A3, and 47G9 as templates. About 250 variants in the combinatorial mutagenesis library were isolated and screened for improved activity and enantioselectivity. About 50% variants displayed improved activity as compared to *Kp*ADH and enantioselectivity of over 90% *ee* (Figure 1I and Table S11). The *ee* values of 49A7 (M131V/F197T/E214Y/S237A), 49D6 (C165W/E214Y/S237A/Q238C), 50C10 (C165F/E214Y/S237A), and 51E10 (M131A/C165F/F197T/E214Y/S237A) were 98.9%, 98.9%, 99.4%, and 98.7%, higher than the variants isolated from Poc_S or Poc_L libraries. Remarkably, 50C10 exhibited the highest *ee* of 99.4% which satisfies the optical purity requirement of pharmaceutical intermediates.[23] Although some variants also display high enantioselectivity, such as 50D8 (M131A/C165F/F197T/E214Y/S237A/Q238C) with 99.5% *ee*, they were eliminated due to lower specific activities than *Kp*ADH.

Kinetic Parameters and MD Simulation Analysis. To get insight into the effect of substrate binding pockets on the improved enantioselectivity, all the beneficial variants were purified to homogeneity, and their kinetic parameters were determined. Several single mutants including M131V, C165F, F197T, E214Y, S237A, and Q238C were also constructed. The K_M, V_{max}, and k_{cat}/K_M of *Kp*ADH were 0.78 mM, 19.8 μmol·

DOI: 10.1021/acscatal.8b02286
ACS Catal. 2018, 8, 8336−8345

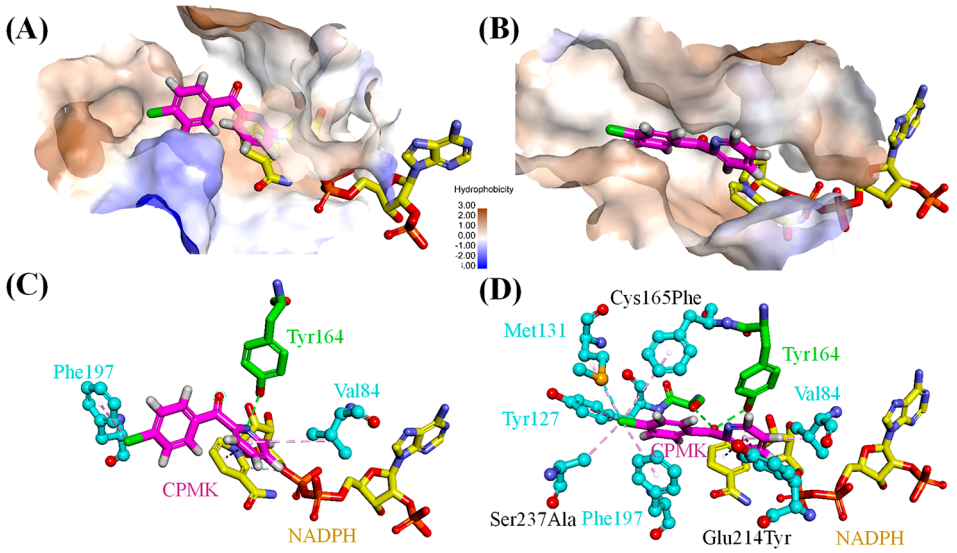

Figure 2. Analysis of substrate binding pockets and interactions between ligand and protein in 20 ns MD simulation of *Kp*ADH and 50C10. (A) Substrate binding pocket of *Kp*ADH. (B) Substrate binding pocket of 50C10. (C) Interactions formed in the average conformation of *Kp*ADH–CPMK. (D) Interactions formed in the average conformation of 50C10-CPMK. CPMK is depicted in magenta, NADPH in yellow, catalytic triad in green, residues of binding pockets in cyan. Hydrogen bond is illustrated in green dotted line, $\pi-\pi$ stacking interaction in magenta line, halogen–alkyl interaction in pink line.

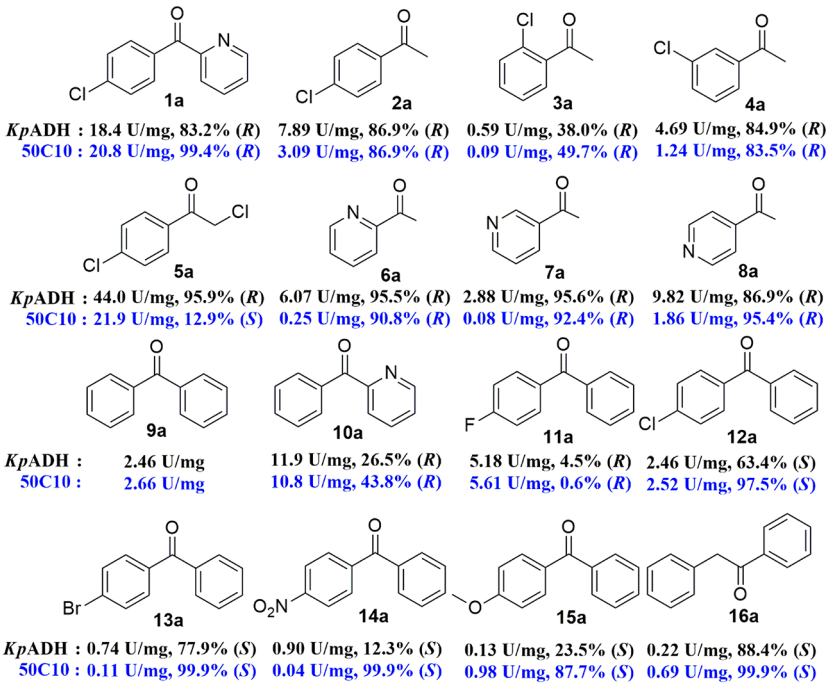

Figure 3. Substrate spectrum of *Kp*ADH and 50C10 toward various prochiral ketones.

$min^{-1}\cdot mg^{-1}$, and 16.9 $s^{-1}\cdot mM^{-1}$, respectively. Variants of Poc_L displayed decreased k_{cat}/K_M as compared with *Kp*ADH due to their higher K_M (Table 2). Among M131V, F197T, and S237A, mutation at F197 exhibited a negative effect on substrate binding affinity, and the K_M of F197T was as high as 8.12 mM, over 10 times that of *Kp*ADH. Similarly, the K_M of 3D3 and 3H8 was also higher than that of *Kp*ADH. The k_{cat}/K_M of 43D11, 45A3, and 47G9 were 10.4, 22.0, and 9.06 $s^{-1}\cdot mM^{-1}$, respectively. The decreased k_{cat}/K_M of 43D11 and 47G9 could be ascribed to the mutation of Q238C since the K_M and k_{cat} of C165F, E214Y, and Q238C were 0.52 mM and 9.26 s^{-1}, 0.80 mM and 14.8 s^{-1}, and 3.42 mM and 10.2 s^{-1}. A similar phenomenon was also found with 49A7, 49D6, and 51E10. Although the k_{cat} values of 49A7, 49D6, and 51E10 were 28.4, 22.0, and 55.4 s^{-1}, much higher than 13.2 s^{-1} of *Kp*ADH, the increased K_M led to lower k_{cat}/K_M, considering all of them contain F197T and (or) Q238C. Both F197T and Q238C play important roles in influencing enantioselectivity; the *ee* values of 3D3 and 47G9 were slightly higher than those of 3H8 and 45A3 as shown in Table 2. The k_{cat}/K_M of the best variant 50C10 (C165F/E214Y/S237A) was 59.3 $s^{-1}\cdot mM^{-1}$, 3.51-fold that of *Kp*ADH, indicating the two-round screening was effective in identifying variants with high activity and enantioselectivity. The *ee* values of C165F, E214Y, and

DOI: 10.1021/acscatal.8b02286
ACS Catal. 2018, 8, 8336–8345

S237A were 89.1%, 94.2%, and 96.1%, while their k_{cat}/K_M values were 17.8, 18.6, and 40.5 $s^{-1}\cdot mM^{-1}$. The results indicate synergistic effects existed among C165, E214, and S237, since 50C10 displayed higher *ee* and k_{cat}/K_M than three single mutants C165F, E214Y, and S237A.

To understand the molecular mechanism of improved enantioselectivity, the crystal structure of *Kp*ADH in complex with NADPH was resolved by X-ray diffraction and was deposited in the Protein Data Bank (PDB) under accession number of 5Z2X (unpublished data). *Kp*ADH is a homodimer enzyme made up of 12 β-sheet surrounded by 10 α-helix (Figure S2). The homology model of 50C10 was constructed by virtual mutation of *Kp*ADH. As illustrated in Figure 2, the substrate binding pocket of 50C10 is enlarged, and the surface becomes more hydrophobic than that of *Kp*ADH. Furthermore, substrate CPMK (**1a**) was docked into *Kp*ADH and 50C10, and the protein−ligand complexes were subjected to 20 ns molecular dynamic (MD) simulation (Figures S3−S4). The average conformations of *Kp*ADH−CPMK and 50C10−CPMK under catalytic state were extracted. The binding free energy between 50C10 and CPMK in the average conformation was calculated to be −103.7 $kcal\cdot mol^{-1}$, which is −31.2 $kcal\cdot mol^{-1}$ lower than that of *Kp*ADH−CPMK. The significantly reduced substrate binding energy could explain the decreased K_M and increased k_{cat} of 50C10. Interactions analysis reveals that only weak interactions could be formed between F197/V84 and CPMK in *Kp*ADH (Figure 2C). However, in 50C10, more nonbonded interactions emerged, including halogen−alkyl interactions between M131/S237A and chlorine-substitute of CPMK and $\pi-\pi$ interactions between E214Y and pyridyl of CPMK as well as C165F and phenyl of CPMK (Figure 2D, Figure S5−S6). In addition, the increased difference between size of Poc_S and Poc_L is also important for the enantioselective recognition. The above analysis indicates that the stereoselectivity of the newly evolved 50C10 was enhanced by reshaping its substrate binding pocket employing HCSM strategy.

Substrate Spectrum of *Kp*ADH and 50C10. Various prochiral ketones with similar substituents as CPMK (**1a**) were chosen to evaluate the substrate specificity of *Kp*ADH and 50C10 as illustrated in Figure 3. For the reduction of chloroacetophenone derivatives (**2a**−**5a**), the specific activities and enantioselectivities of 50C10 were relatively lower than those of *Kp*ADH and in an order of 4′-chloroacetophenone > 3′-chloroacetophenone > 2′-chloroacetophenone. A similar phenomenon was also observed in the reduction of different acetylpyridines (**6a**−**8a**), except for 1-(pyridin-4′-yl)ethanone (**8a**). These results confirmed the importance of 2′-pyridyl and 4′-chlorophenyl groups in influencing the recognition and binding of **1a** by *Kp*ADH. Eight diaryl ketones (**9a**−**16a**) were also selected to investigate the substrate profiles. Unlike chloroacetophenones or acetylpyridines, 50C10 displayed improved specific activities and enantioselectivities to almost all tested diaryl ketones. The specific activities of 50C10 toward **9a**, **11a**, **12a**, **15a**, and **16a** were 1.02−7.54-fold that of *Kp*ADH. The *ee* values of 50C10 were significantly increased, especially toward **12a** (97.5%, *S*), **13a** (99.9%, *S*), **14a** (99.9%, *S*), **15a** (87.7%, *S*), and **16a** (99.9%, *S*) with large electron-withdrawing substituents at para position, much higher than 12.3%−88.4% (*S*) of *Kp*ADH. Consequently, variant 50C10 could be potentially applied in the synthesis of optically pure diaryl alcohols with halogen or other electron-withdrawing substituents.

Asymmetric Preparation of Chiral (*R*)-1b Employing Variant 50C10. Considering its highest enantioselectivity and catalytic efficiency, 50C10 was applied in asymmetric reduction of CPMK (**1a**) for producing (*R*)-CPMA ((*R*)-**1b**) at high substrate loading (Figure 4). Glucose dehydrogenase

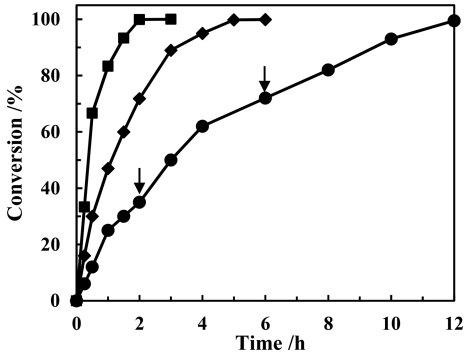

Figure 4. Asymmetric preparation of (*R*)-CPMA employing 50C10 at different substrate loadings: (■) 100 mM, (♦) 200 mM, (●) 500 mM, (↓) addition of 200 mM and 100 mM substrate at 2.0 and 6.0 h. Reactions were performed with 0.30 and 0.10 g dry cell weight of 50C10 and GDH, 2.0−10.0 mmol CPMK dissolved in 2 mL ethanol, and 3.0−7.5 mmol glucose in 18 mL Tris-HCl (pH 7.5, 100 mM), magnetically agitated at 200 rpm and 30 °C and maintained at pH 7.5 using 1.0 M NaOH. Samples were withdrawn at different time intervals and analyzed by HPLC equipped with chiral OB-H column at 254 nm.

from *Bacillus megaterium* (*Bm*GDH) was introduced for cofactor regeneration. Tris-HCl (pH 7.5, 100 mM) was used as reaction buffer in which 50C10 and *Bm*GDH retained relatively matched activities. As an initial attempt, 100 mM **1a** (21.7 $g\cdot L^{-1}$) with 10% ethanol as cosolvent was completely converted into (*R*)-**1b** within 2 h. Then, the substrate concentration was increased to 200 mM **1a** (43.4 $g\cdot L^{-1}$) with the same amount of enzymes. The conversion rate reached 72.1% at 2 h, and a full conversion was achieved at 6 h with 99.5% *ee* and no external $NADP^+$. Considering the superior enantioselectivity and substrate tolerance of 50C10 compared with other reported diaryl ketone reductases, much higher substrate loading was also investigated.[7] Due to the low solubility of **1a**, fed-batch of substrate was employed. As shown in Figure 4, 4.0, 4.0, and 2.0 mmol of **1a** were added into the reaction mixture (a final concentration of 500 mM) at 0, 2, and 6 h. After 12 h of agitation, **1a** was fully reduced with conversion of 99.7% and 99.4% *ee*. After extraction with ethyl acetate and evaporation under vacuum, about 1.94 g of white powder of (*R*)-**1b** was obtained with an isolation yield of 88.6%. The space−time yield reached 194 $g\cdot L^{-1}\cdot d^{-1}$ without assistance of external $NADP^+$. The product was confirmed by NMR analysis (Figure S37−S38): ^1H NMR (400 MHz, $CDCl_3$) δ 5.34 (s, 1H), 5.74 (s, 1H), 7.14 (d, J = 7.9 Hz, 1H), 7.23 (dd, J_1 = 7.1 Hz, J_2 = 5.1 Hz, 1H), 7.29−7.38 (m, 4H), 7.65 (td, J_1 = 7.7 Hz, J_2 = 1.7 Hz, 1H), 8.58 (d, J = 4.8 Hz, 1H); ^{13}C NMR (75 MHz, $CDCl_3$) δ 160.93, 148.00, 141.79, 137.12, 133.47, 128.68, 128.37, 122.65, 121.19, 77.66, 77.23, 76.81, 74.58. To the best of our knowledge, this is the first report on the bioreductive synthesis of chiral antihistamine precursor (*R*)-CPMA with >99% *ee* and over 100 $g\cdot L^{-1}$ substrate loading.

DOI: 10.1021/acscatal.8b02286
ACS Catal. 2018, 8, 8336−8345

CONCLUSIONS AND PERSPECTIVES

In summary, hydroclassified combinatorial saturation mutagenesis (HCSM) was proposed and applied in the directed evolution of enantioselectivity of alcohol dehydrogenase *Kp*ADH. Using this smart HCSM strategy, the library size could be significantly reduced especially with simultaneous mutation of three or more residues. The interactions including hydrophobicity and steric hindrance in the substrate binding pocket could be properly balanced employing the HCSM strategy by dividing 20 amino acids into four groups. Six hotspots critical for the enantioselectivity were identified in the substrate binding pockets of *Kp*ADH by alanine/tyrosine scanning. After two rounds of screening, a highly enantioselective variant 50C10 was identified among 5500 variants. 50C10 displayed high binding affinity and catalytic efficiency with k_{cat}/K_M of 59.3 $s^{-1}\cdot mM^{-1}$, 3.51-fold that of *Kp*ADH. Hydrophobic interaction in large substrate binding pocket and steric hindrance in small substrate binding pocket were proposed to be the main mechanisms for the improved enantioselectivity as proved by MD simulation. Substrate spectrum analysis revealed that 50C10 preferred diaryl ketones and displayed improved enantioselectivity, especially toward diaryl ketones with halogen or other electron-withdrawing substituents. Variant 50C10 also demonstrated high efficacy and substrate tolerance in the preparation of chiral diaryl alcohols and could convert as much as 0.5 M (108.5 $g\cdot L^{-1}$) (4-chlorophenyl)-(pyridin-2-yl)-methanone with 99.4% *ee* and space−time yield of 194 $g\cdot L^{-1}\cdot d^{-1}$ without external $NADP^+$. This newly proposed HCSM strategy could be potentially applied in the directed evolution of activity, substrate spectrum, and enantioselectivity especially when lacking of high throughput screening methods. This study also provides a highly efficient and enantioselective ketoreductase for the preparation of chiral diaryl alcohols.

MATERIALS AND METHODS

General Remarks. Plasmid pET28-*kpadh* was constructed in our previous work. Prochiral ketones, (4′-chlorophenyl)-(pyridin-2-yl)methanone (**1a**), 4′-chloroacetophenone (**2a**), 2′-chloroacetophenone (**3a**), 3′-chloroacetophenone (**4a**), 2-chloro-1-(4′-chlorophenyl)ethanone (**5a**), 1-(pyridin-2′-yl)-ethanone (**6a**), 1-(pyridin-3′-yl)ethanone (**7a**), 1-(pyridin-4′-yl)ethanone (**8a**), benzophenone (**9a**), (pyridin-2′-yl)-phenylmethanone (**10a**), (4′-fluorophenyl)phenylmethanone (**11a**), (4′-chlorophenyl)phenylmethanone (**12a**), (4′-bromophenyl)phenylmethanone (**13a**), (4′-nitrophenyl)-phenylmethanone (**14a**), (4′-methoxyphenyl)-phenylmethanone (**15a**), and 1,2-diphenylethanone (**16a**) were purchased from Aladdin Inc.. NADPH was bought from Merck Inc.

Site-Directed Mutagenesis and Protein Expression. Site-directed mutagenesis of alanine/tyrosine scanning was conducted by whole plasmid PCR using Phanta Super-Fidelity DNA Polymerase (Vazyme Inc.). Primers are listed in Table S1. PCR procedure was predenaturation at 96 °C for 5 min, 15 cycles of denaturation at 98 °C for 20 s, annealing at 50−65 °C for 20 s and elongation at 68 °C for 210 s, and final elongation at 68 °C for 10 min. The resultant PCR products were digested with *Dpn*I to remove the parental pET28-*kpadh*. Furthermore, 5.0 μL of digested products were transformed into *E. coli* BL21(DE3). Expression of the *Kp*ADH variants was induced with 0.2 mM IPTG at 25 °C for 6 h as previously reported.

Activity Assay and Enantioselectivity Determination. The activity of *Kp*ADH variants was spectrophotometrically determined according to the optical changes of NADPH at 340 nm and 30 °C. Assay mixture contained 2.0 mM CPMK, 0.5 mM NADPH, and 10 μL enzyme in PBS buffer (100 mM, pH 6.0). One unit of activity was defined as the amount of enzyme required for the depletion of 1.0 μmol NADPH at the above-mentioned condition. Enantioselectivity was calculated according to the peak area of (*R*)- and (*S*)-CPMA determined by chiral HPLC equipped with Chiralcel OB-H column (4.6 mm × 250 mm × 5 μm, Daicel Chiral Technologies Co., Ltd.) as previously reported. All the assays were performed in triplicate.

Construction and Screening of HCSM Libraries. Overlap extension PCR was adopted to obtain the whole *Kp*ADH product with three mutational sites. Furthermore, the products were ligated into linearized pET28a by ClonExpress II (Vazyme Inc.). The resultant recombinant plasmids containing multiple mutations at M131/F197/S237 or C165/E214/Q238 were transformed into *E. coli* BL21(DE3). Different pairs of primers were used to form different HCSM libraries, and all the primers are listed in Table S2. About 600 monocolonies in each HCSM library were screened to achieve 95% coverage. Then all the strains were inoculated into 96-deep well plates and cultivated as above-mentioned for the expression of *Kp*ADH variants. After centrifugation, cells were freeze−thawed at −80 °C followed by lysozyme and DNaseI treatment to obtain crude extracts. Two rounds of screening were adopted. First, the activities of all the variants were high throughout determined as above-mentioned. Then, the enantioselectivities of variants with similar or higher activity than *Kp*ADH were determined.

Protein Purification and Preparation of Crude Enzyme Powder. *Kp*ADH and variants with His-tag were purified to homogeneity by nickel-affinity chromatography as previously reported and analyzed by SDS-PAGE. Fermentation of 50C10 was carried out with 2 × LB as fermentation medium. Cells harboring 50C10 were harvested, washed with physiological saline, and disrupted with nanohomogenize machine (ATS AH-BASICI). The crude extract was obtained by centrifugation and lyophilized under vacuum (SCIENTZ-10N) to form the crude enzyme powder, which was stored at 4 °C for further use.

Determination of Kinetic Parameters and Substrate Profiles. Kinetic parameters of *Kp*ADH and variants were determined. The specific activities of each variant toward 0.1−5.0 mM **1a** were assayed employing the above-mentioned protocol. K_M, V_{max}, and k_{cat} were calculated according to the Lineweaver−Burk plot. Substrate profiles of *Kp*ADH and 50C10 were measured toward prochiral ketones **1a**−**16a**. The final substrate concentration of each substrates was 2.0 mM. The analytical methods for enantioselectivity of all tested substrates are summarized in Table S12. All the activities and enantioselectivities were measured in triplicate.

Asymmetric Preparation of Chiral (*R*)-CPMA. Asymmetric reduction of **1a** for the preparation of (*R*)-CPMA was performed with 0.30 and 0.10 g of crude enzyme powder of 50C10 and GDH, 2.0−10.0 mmol **1a** dissolved in 2 mL of ethanol, and 3.0−7.5 mmol glucose in 18 mL of Tris-HCl (pH 7.5, 100 mM). Reactions were magnetically agitated at 200 rpm and 30 °C and maintained at pH 7.5 using 1.0 M NaOH. Samples were withdrawn from the reaction mixture at different time points, and the conversion and enantioselectivity were analyzed as above-mentioned. After the reaction, the mixture

DOI: 10.1021/acscatal.8b02286
ACS Catal. 2018, 8, 8336−8345

was extracted three times with ethyl acetate. The organic phase was combined and dried over anhydrous Na_2SO_4. Furthermore, the organic phase was evaporated under vacuum to obtain (*R*)-**1b** as white powder.

Homology Modeling and Molecular Docking Analysis. Protein modeling was implemented with EasyModeller 4.0 using protein structures 4PVC and 5B6K as templates and verified with SAVES (Structure Analysis and Verification Server version 4). All docking calculations were accomplished with AutoDock Vina 1.1, with the docking algorithm that took account of ligand flexibility but kept the protein rigid. Docking runs were carried out using standard parameters of the program for interactive growing and subsequent scoring. Molecular dynamic simulation was carried out employing the NAMD module of Discover Studio 3.5. CHARMm force field and temperature of 300 K were adopted, and the simulation time was set as 20 ns. Stereoviews were constructed using Pymol.

■ ASSOCIATED CONTENT

Supporting Information

The Supporting Information is available free of charge on the ACS Publications website at DOI: 10.1021/acscatal.8b02286.

Supporting tables and figures for primers, creation and screening of HCSM libraries, enantioselectivity analysis, original data of kinetic parameters and substrate profiles, ^{1}H NMR and ^{13}C NMR of synthesized (*R*)-CPMA, and crystal structure of *Kp*ADH (5Z2X) (PDF)

■ AUTHOR INFORMATION

Corresponding Author

*E-mail: yni@jiangnan.edu.cn.

ORCID

Ye Ni: 0000-0003-4887-7517

Notes

The authors declare no competing financial interest.

■ ACKNOWLEDGMENTS

We are grateful to the National Natural Science Foundation of China (21506073, 21776112), the Natural Science Foundation of Jiangsu Province (BK20150003, BK20171135), Six Talent Peaks project of Jiangsu Province (2015-SWYY-008), the Program of Introducing Talents of Discipline to Universities (111-2-06), the national first-class discipline program of Light Industry Technology and Engineering (LITE2018-07), and a project funded by the Priority Academic Program Development of Jiangsu Higher Education Institutions for the financial support of this research.

■ REFERENCES

(1) (a) Barouh, V.; Dall, H.; Patel, D.; Hite, G. Stereochemical Aspects of Antihistamine Action. 4. Absolute Configuration of Carbinoxamine Antipodes. *J. Med. Chem.* **1971**, *14*, 834−836. (b) Meguro, K.; Aizawa, M.; Sohda, T.; Kawamatsu, Y.; Nagaoka, A. New 1,4-Dihydropyridine Derivatives with Potent and Long-Lasting Hypotensive Effect. *Chem. Pharm. Bull.* **1985**, *33*, 3787−3797. (c) Casy, A. F.; Drake, A. F.; Ganellin, C. R.; Mercer, A. D.; Upton, C. Stereochemical Studies of Chiral H-1 Antagonists of Histamine: The Resolution, Chiral Analysis, and Biological Evaluation of Four Antipodal Pairs. *Chirality* **1992**, *4*, 356−366. (d) Farina, V.; Reeves, J. T.; Senanayake, C. H.; Song, J. J. Asymmetric Synthesis of Active Pharmaceutical Ingredients. *Chem. Rev.* **2006**, *106*, 2734−2793.

(2) (a) Botta, M.; Summa, V.; Corelli, F.; Di Pietro, G. D.; Lombardi, P. Synthesis of Aryl 2-Benzofuranyl- and 2-Indolyl(aryl)-carbinols of High Enantiomeric Purity via Palladium-catalyzed Heteroannulation of Chiral Arylpropargylic Alcohols. *Tetrahedron: Asymmetry* **1996**, *7*, 1263−1266. (b) Jen, W. S.; Truppo, M. D.; Amos, D.; Devine, P.; McNevin, M.; Biba, M.; Campos, K. Copper-catalyzed Synthesis of Enantioenriched Tetraarylethanes. *Org. Lett.* **2008**, *10*, 741−744.

(3) (a) Hashiguchi, S.; Fujii, A.; Takehara, J.; Ikariya, T.; Noyori, R. Asymmetric Transfer Hydrogenation of Aromatic Ketones Catalyzed by Chiral Ruthenium(II) Complexes. *J. Am. Chem. Soc.* **1995**, *117*, 7562−7563. (b) Yang, H. L.; Huo, N. N.; Yang, P.; Pei, H.; Lv, H.; Zhang, X. M. Rhodium Catalyzed Asymmetric Hydrogenastion of 2-Pyridine Ketones. *Org. Lett.* **2015**, *17*, 4144−4147. (c) Touge, T.; Nara, H.; Fujiwhara, M.; Kayaki, Y.; Ikariya, T. Efficient Access to Chiral Benzhydrols via Asymmetric Transfer Hydrogenation of Unsymmetrical Benzophenones with Bifunctional Oxo-tethered Ruthenium Catalysts. *J. Am. Chem. Soc.* **2016**, *138*, 10084−10087.

(4) (a) Bornscheuer, U. T.; Huisman, G. W.; Kazlauskas, R. J.; Lutz, S.; Moore, J. C.; Robins, K. Engineering the Third Wave of Bocatalysis. *Nature* **2012**, *485*, 185−194. (b) Honig, M.; Sondermann, P.; Turner, N. J.; Carreira, E. M. Enantioselective Chemo- and Biocatalysis: Partners in Retrosynthesis. *Angew. Chem., Int. Ed.* **2017**, *56*, 8942−8973. (c) Sheldon, R. A.; Woodley, J. M. Role of Biocatalysis in Sustainable Chemistry. *Chem. Rev.* **2018**, *118*, 801−838.

(5) (a) Ma, S. K.; Gruber, J.; Davis, C.; Newman, L.; Gray, D.; Wang, L.; Grate, J.; Huisman, G. W.; Sheldon, R. A. A Green-by-Design Biocatalytic Process for Atorvastatin Intermediate. *Green Chem.* **2010**, *12*, 81−86. (b) Savile, C. K.; Janey, J. M.; Mundorff, E. C.; Moore, J. C.; Tam, S.; Jarvis, W. R.; Colbeck, J. C.; Krebber, A.; Fleitz, F. j.; Brands, J.; Devine, P. N.; Huisman, G. W.; Hughes, G. J. Biocatalytic Asymmetric Synthesis of Chiral Amines from Ketones Applied to Sitagliptin Manufacture. *Science* **2010**, *329*, 305−309.

(6) (a) Chartrain, M.; Lynch, J.; Choi, W. B.; Churchill, H.; Patel, S.; Yamazaki, S.; Volante, R.; Greasham, R. Asymmetric Bioreduction of a Bisaryl Ketone to its Corresponding (*S*)-Bisaryl Alcohol, by the Yeast *Rhodotorula pilimanae* ATCC 32762. *J. Mol. Catal. B: Enzym.* **2000**, *8*, 285−288. (b) Ni, Y.; Zhou, J. Y.; Sun, Z. H. Production of a Aey Chiral Intermediate of Betahistine with a Newly Isolated *Kluyveromyces* sp. in an Aqueous Two-Phase System. *Process Biochem.* **2012**, *47*, 1042−1048. (c) Xu, J. X.; Zhou, S. Y.; Zhao, Y. J.; Xia, J.; Liu, X. Y.; Xu, J. M.; He, B. F.; Wu, B.; Zhang, J. F. Asymmetric Whole-Cell Bioreduction of Sterically Bulky 2-Benzoylpyridine Derivatives in Aqueous Hydrophilic Ionic Liquid Media. *Chem. Eng. J.* **2017**, *316*, 919−927.

(7) (a) Truppo, M. D.; Pollard, D.; Devine, P. Enzyme-Catalyzed Enantioselective Diaryl Ketone Reductions. *Org. Lett.* **2007**, *9*, 335−338. (b) Li, H. M.; Zhu, D. M.; Hua, L.; Biehl, E. R. Enantioselective Reduction of Diaryl Ketones Catalyzed by a Carbonyl Reductase from *Sporobolomyces salmonicolor* and its Mutant Enzymes. *Adv. Synth. Catal.* **2009**, *351*, 583−588.

(8) Zhou, J. Y.; Xu, G. C.; Han, R. Z.; Dong, J. J.; Zhang, W. G.; Zhang, R. Z.; Ni, Y. Carbonyl Group-Dependent High-Throughput Screening and Enzymatic Characterization of Diaromatic Ketone Reductase. *Catal. Sci. Technol.* **2016**, *6*, 6320−6327.

(9) (a) Davids, T.; Schmidt, M.; Bottcher, D.; Bornscheuer, U. T. Strategies for the Discovery and Engineering of Enzymes for Biocatalysis. *Curr. Opin. Chem. Biol.* **2013**, *17*, 215−220. (b) Reetz, M. T. Biocatalysis in Organic Chemistry and Biotechnology: Past, Present, and Future. *J. Am. Chem. Soc.* **2013**, *135*, 12480−12496. (c) Denard, C. A.; Ren, H. Q.; Zhao, H. M. Improving and Repurposing Biocatalysts via Directed Evolution. *Curr. Opin. Chem. Biol.* **2015**, *25*, 55−64. (d) Arnold, F. H. Directed Evolution: Bringing New Chemistry to Life. *Angew. Chem., Int. Ed.* **2018**, *57*, 4143−4148.

(10) (a) Reetz, M. T.; Bocola, M.; Carballeira, J. D.; Zha, D.; Vogel, A. Expanding the Range of Substrate Acceptance of Enzymes: Combinatorial Active-Site Saturation Test. *Angew. Chem., Int. Ed.* **2005**, *44*, 4192−4196. (b) Bougioukou, D. J.; Kille, S.; Taglieber, A.;

DOI: 10.1021/acscatal.8b02286
ACS Catal. 2018, 8, 8336−8345

Reetz, M. T. Directed Evolution of an Enantioselective Eoate-Reductase: Testing the Utility of Iterative Saturation Mutagenesis. *Adv. Synth. Catal.* **2009**, *351*, 3287−3305.
(11) (a) Neylon, C. Chemical and Biochemical Strategies for the Randomization of Protein Encoding DNA Sequences: Library Construction Methods for Directed Evolution. *Nucleic Acids. Res.* **2004**, *32*, 1448−1459. (b) Shivange, A. V.; Marienhagen, J.; Mundhada, H.; Schenk, A.; Schwaneberg, U. Advances in Generating Functional Diversity for Directed Protein Evolution. *Curr. Opin. Chem. Biol.* **2009**, *13*, 19−25. (c) Reetz, M. T.; Krebs, G. P. L. Challenges in the Directed Evolution of Stereoselective Enzymes for Use in Organic Chemistry. *C. R. Chim.* **2011**, *14*, 811−818. (d) Feng, X. J.; Sanchis, J.; Reetz, M. T.; Rabitz, H. Enhancing the Efficiency of Directed Evolution in Focused Enzyme Libraries by the Adaptive Substituent Reordering Algorithm. *Chem. - Eur. J.* **2012**, *18*, 5646−5654. (e) Reetz, M. T. Laboratory Evolution of Stereoselective Enzymes as a Means to Expand the Toolbox of Organic Chemists. *Tetrahedron* **2012**, *68*, 7530−7548.
(12) (a) Lutz, S.; Patrick, W. M. Novel Methods for Directed Evoltuion of Enzymes: Quality, not Quantity. *Curr. Opin. Biotechnol.* **2004**, *15*, 291−297. (b) Pines, G.; Pines, A.; Garst, A. D.; Zeitoun, R. I.; Lynch, S. A.; Gill, R. T. Codon Compression Algorithms for Saturation Mutagenesis. *ACS Synth. Biol.* **2015**, *4*, 604−614.
(13) (a) Reetz, M. T. Laboratory Evolution of Stereoselective Enzymes: A Profilic Source of Catalysts for Asymmetric Reactions. *Angew. Chem., Int. Ed.* **2011**, *50*, 138−174. (b) Reetz, M. T.; Kahakeaw, D.; Lohmer, R. Addressing the Numbers Problem in Directed Evolution. *ChemBioChem* **2008**, *9*, 1797−1804.
(14) (a) Kamtekar, S.; Schiffer, J. M.; Xiong, H.; Babik, J.; Hecht, M. H. Protein Design by Binary Patterning or Polar and Nonpolar Amino Acids. *Science* **1993**, *262*, 1680−1685. (b) Roy, S.; Hecht, M. H. Cooperative Thermal Denaturation of Proteins Designed by Binary Patterning of Polar and Nonpolar Amino Acids. *Biochemistry* **2000**, *39*, 4603−4607. (c) Sun, Z. T.; Salas, P. T.; Siirola, E.; Lonsdale, R.; Reetz, M. T. Exploring Productive Sequence Space in Directed Evolution Using Binary Patterning versus Conventional Mutagenesis Strategies. Bioresour. *Bioprocessing* **2016**, *3*, 44. (d) Li, G. Y.; Reetz, M. T. Learning Lessons from Directed Evolution of Stereoselective Enzymes. *Org. Chem. Front.* **2016**, *3*, 1350−1358. (e) Reetz, M. T. Combinatorial Libraries Reloaded. *Isr. J. Chem.* **2018**, *58*, 52−60.
(15) (a) Hughes, M. D.; Nagel, D. A.; Santos, A. F.; Sutherland, A. J.; Hine, A. V. Removing the Redundancy from Randomized GeneLibraries. *J. Mol. Biol.* **2003**, *331*, 973−979. (b) Reetz, M. T.; Wu, S. Greatly Reduced Amino Acid Alphabets in Directed Evolution: Making the Right Choice for Saturation Mutagenesis at Homologous Enzyme Position. *Chem. Commun.* **2008**, *43*, 5499−5501. (c) Reetz, M. T.; Prasad, S.; Carballeira, J. D.; Gumulya, Y.; Bocola, M. Iterative Saturation Mutagenesis Accelerates Laboratory Evolution of Enzyme Stereoselectivity: Rigorous Comparison with Traditional Methods. *J. Am. Chem. Soc.* **2010**, *132*, 9144−9152. (d) Kille, S.; Acevedo-Rocha, C. G.; Parra, L. P.; Zhang, Z. G.; Opperman, D. J.; Reetz, M. T.; Acevedo, J. P. Reducing Codon Redundancy and Screening Effort of Combinatorial Protein Libraries Created by Saturation Mutagenesis. *ACS Synth. Biol.* **2013**, *2*, 83−92.
(16) (a) Sun, Z. T.; Lonsdale, R.; Kong, X. D.; Xu, J. H.; Zhou, J. H.; Reetz, M. T. Reshaping an Enzyme Binding Pocket for Enhanced and Inverted Stereoselectivity: Use of Smallest Amino Acid Alphabets in Directed Evolution. *Angew. Chem., Int. Ed.* **2015**, *54*, 12410−12415. (b) Sun, Z. T.; Lonsdale, R.; Wu, L.; Li, G. Y.; Li, A. T.; Wang, J. B.; Zhou, J. H.; Reetz, M. T. Structure-Guided Triple Code Saturation Mutagenesis: Efficient Tuning of the Stereoselectivity of an Epoxide Hydrolase. *ACS Catal.* **2016**, *6*, 1590−1597. (c) Sun, Z. T.; Lonsdale, R.; Ilie, A.; Li, G. Y.; Zhou, J. H.; Reetz, M. T. Catalytic Asymmetric Reduction of Difficult-to-Reduce Ketones: Triple Code Saturation Mutagenesis of Alcohol Dehydrogenase. *ACS Catal.* **2016**, *6*, 1598−1605.
(17) Zhao, J.; Kardashliev, T.; Ruff, A. J.; Bocola, M.; Schwaneberg, U. Lessons from Diversity of Directed Evolution Experiments by an Analysis of 3,000 Mutations. *Biotechnol. Bioeng.* **2014**, *111*, 2380−2389.
(18) (a) Filling, C.; Berndt, K. D.; Benach, J.; Knapp, S.; Prozorovski, T.; Nordling, E.; Ladenstein, R.; Jörnvall, H.; Oppermann, U. Critical Residues for Structure and Catalysis in Short-Chain Dehydrogenases/Reductases. *J. Biol. Chem.* **2002**, *277*, 25677−25684. (b) Deng, J.; Yao, Z. Q.; Chen, K. L.; Yuan, Y. A.; Lin, J. P.; Wei, D. Z. Towards the Computational Design and Engineering of Enzyme Enantioselectivity: A CaseStudy by a Carbonyl Reductase from. *J. Biotechnol.* **2016**, *217*, 31−40.
(19) (a) Schlieben, N. H.; Niefind, K.; Müller, J.; Riebel, B.; Hummel, W.; Schomburg, D. Atomic Resolution Structures of *R*-Specific Alcohol Dehydrogenase from *Lactobacillus brevis* Provide the Structural Bases of its Substrate and Cosubstrate Specificity. *J. Mol. Biol.* **2005**, *349*, 801−813. (b) Noey, E. L.; Tibrewal, N.; Jiménez-Osés, G.; Osuna, S.; Park, J. Y.; Bond, C. M.; Cascio, D.; Liang, J.; Zhang, X. Y.; Huisman, G. W.; Tang, Y.; Houk, K. N. Origins of Stereoselectivity in Evolved Ketoreductases. *Proc. Natl. Acad. Sci. U. S. A.* **2015**, *112*, E7065−E7072.
(20) (a) Guo, P. C.; Bao, Z. Z.; Ma, X. X.; Xia, Q.; Li, W. F. Structural Insights into the Cofactor-Assisted Substrate Recognition of Yeast Methylglyoxal/isovaleraldehyde Reductase Gre2. *Biochim. Biophys. Acta, Proteins Proteomics* **2014**, *1844*, 1486−1492. (b) Qin, F. Y.; Qin, B.; Mori, T.; Wang, Y.; Meng, L. X.; Zhang, X.; Jia, X.; Abe, I.; You, S. Engineering of *Candida glabrata* Ketoreductase 1 for Asymmetric Reduction of Alpha-halo Ketones. *ACS Catal.* **2016**, *6*, 6135−6140.
(21) Cunningham, B. C.; Wells, J. A high-Resolution Epitope Mapping of hGH-Receptor Interactions by Aanine-Scanning Mutagenesis. *Science* **1989**, *244*, 1081−1085.
(22) (a) Sun, Z. T.; Lonsdale, R.; Li, G. Y.; Reetz, M. T. Comparing Different Strategies in Directed Evolution of Enzyme Stereoselectivity: Single- versus Double-Codon Saturation Mutagenesis. *ChemBioChem* **2016**, *17*, 1865−1872. (b) Sun, Z. T.; Wikmark, Y.; Backvall, J. E.; Reetz, M. T. New Concepts for Increasing the Efficiency in Directed Evolution of Stereoselective Enzymes. *Chem. - Eur. J.* **2016**, *22*, 5046−5054.
(23) Luetz, S.; Giver, L.; Lalonde, J. Engineered Enzymes for Chemical Production. *Biotechnol. Bioeng.* **2008**, *101*, 647−653.

DOI: 10.1021/acscatal.8b02286
ACS Catal. 2018, 8, 8336−8345